Egypt. J. Microbiol. **Vol. 57,** pp. 75-87 (2022)

EgyptianJournalofMicrobiology
http://ejm.journals.ekb.eg/

In silico Homology Modeling of Five *Aspergillus oryzae* Extracellular Proteins and Docking with Silver Nanoparticles

Huda AbdelHamid, Marwa Obiedallah[#]
Botany and Microbiology Department, Faculty of Science, Sohag University, Sohag, 82524, Egypt.

THE USE of computational methods for constructing a protein model to support experimental findings aid in answering a great number of questions about the mechanisms underlying various scientific processes. Constructing a protein model and molecular docking computationally can present a clear explanation of biological process integrating to experimental findings. One of the most precise methods currently available is detecting a homolog to a specific amino acid sequence to use it as a template for modeling. In this paper, we present synthesis of 13.6 ± 2.2nm silver nanoparticles using extracellular filtrate of *Aspergillus oryzae* and homology modeling of five targeted extracellular proteins, as well as homology prediction for each protein's active site. In addition, a nanoparticle of silver that docks with all five proteins is evaluated *in silico*. According to the results, only 32 out of 50 top 10 solutions for each protein contained polar oxygen or nitrogen atom neighbors. Seven of the 50 solutions for FAD-dependent oxidoreductase contained the greatest number of detectable polar neighbors (six measurements). This finding supports the hypothesis that extracellular fungal proteins play a crucial role in capping silver nanoparticles at various positions and preventing aggregation and sedimentation of nanoparticles. Through homology modeling and docking, we reveal the interaction between FAD-dependent oxidoreductase and silver nanoparticles for the first time.

Keywords: Binding site, Docking, Homology modeling, PyMOL, Silver nanoparticles.

Introduction

The synthesis of silver nanoparticles (AgNPs) via physical, chemical, and biological means has attracted researchers from various disciplines. Given that silver nanoparticles possess broad-spectrum antimicrobial activity, this is a challenging area of study (Rai et al., 2014; Gupta et al., 2017; Loo et al., 2018).

Due to their simple nutritional needs, cell rigidity, and high rate of protein secretion, fungi have been cited as one of the most efficient biological sources for AgNPs production (Yadav et al., 2015). In addition, nearly 6400 bio-active compounds are reported to be produced by filamentous fungi (*Ascomycetes* and *Deuteromycetes*) and other fungal species, making fungi a promising biological source for research (Bérdy, 2005).

Several fungal species have been tested to produce nanoparticles intra/extracellularly (Yadav et al., 2015). As heterotrophic organisms, fungi secrete enzymes extracellularly and absorb nutrients internally. Therefore, when a fungus is challenged with a metal salt solution, it is expected to overcome this stress and ensure its own survival, it can eventually convert the toxic metal-ion into nontoxic metallic solid nanoparticles (Mehra & Winge, 1991). The heavy-metal tolerance and ability to bio-accumulate metals, gave some microorganisms the high capability of reducing and stabilizing metals (Guilger-Casagrande & Lima, 2019). The biological pathway or mechanism of silver nitrate ($AgNO_3$) absorption by fungi has not yet been reported.

The Food and Drug Administration of the United States classifies *Aspergillus oryzae* as

[#]Corresponding author email: m.obiedallah@science.sohag.edu.eg, ORCID ID: 0000-0002-8359-1664
Received: 22/11/2022; Accepted: 20/02/2023
DOI: 10.21608/EJM.2023.176267.1220

"*generally regarded as safe*" (Matsushita-Morita et al., 2010). Due to its competitiveness against other microorganisms and highly extracellular enzymatic activity (Liang et al., 2009). *Aspergillus oryzae* is widely used in brewing and many important industries. Furthermore, numerous researchers have also reported the biosynthesis of AgNPs (Tarafdar & Raliya, 2013; Bhimba et al., 2015). However, there are currently no reports on the protein structure produced by *A*. *oryzae* and its interaction with AgNPs.

Solving the three-dimensional structure of proteins can aid in the development of hypotheses regarding their biological function and interactions with other proteins or molecules. In addition, the structure of proteins reveals active sites that may constitute the most efficient portion of a biological reaction. Using software and computational methods to predict protein structure is a shortcut to understanding biological processes at the protein level. Experimental techniques such as crystallography and NMR are extremely difficult, expensive, and require experience.

This study presents the homology modeling (comparative modeling) of five extracellular *A*. *oryzae* proteins. Then, we utilized in silico molecular docking as a promising predictor of silver nanoparticle-protein interaction. This suggests that these proteins play a crucial role as reducing/capping agents for silver ions/solids. Through this bioprocess, models were developed to link protein structures with their functions.

Materials and Methods

Strain

A soil sample from an agricultural land at Sohag governorate, Egypt; was obtained for fungal isolation using soil serial dilution method (Warcup, 1950). Using morphological characterization of fungal isolates, filtrate of *Aspergillus oryzae* (Ahlb.) Cohn (local number $AOry_{17}$) was targeted for myco-generation of silver nanoparticles. Fungal filtrate was mixed with $AgNO_3$ solution (1 mM, final concentration) and kept in dark at 28°C for 24h on a rotary shaker at 200 rpm. Formed silver nanoparticles were detected using UV-Vis spectrophotometer and imaged using transmission electron microscopy (TEM).

Dataset of biological active proteins of Aspergillus oryzae

The following five proteins were selected and used as the dataset in the current study: Peptidase M1 membrane alanine aminopeptidase [*Aspergillus oryzae*], gi|OOO14201, Taka-amylase A precursor [*Aspergillus oryzae*], gi|BAA00336; FAD-dependent oxidoreductase [*A. oryzae*], gi|BAK26560; Leucine aminopeptidase A [*Aspergillus oryzae* RIB40], gi|Q2U1F3 and alkaline protease, partial [*Aspergillus oryzae*], gi|BAA00258.

Protein homology modeling and prediction of binding sites

In order to create a three-dimensional model of each protein and determine whether each protein possesses a ligand that utilizes similar structures, 3DLigandSite predicted ligand-binding sites (Wass et al., 2010). This website obtains search results through three major steps. The first step is to submit the query sequence to the Phyre2 web server, which is a server for protein fold recognition (Kelley et al., 2015). he second step identifies bound ligands with homologous structures to the query. MAMMOTH performs a comprehensive structural scan of the modeled structure against a library of protein structures with engaged ligands (Ortiz et al., 2002). The top 25 scoring (using the MAMMOTH-lnE score) structures were used for analysis, and TMalign is used to align the structures with the model (Zhang & Skolnick, 2005). After removing ligands from homologous structures, found ligands were superimposed onto the modeled structure. Lastly, ligands and residues within a distance threshold clustered ligands were portended. The Jensen Shannon divergence score (Capra & Singh, 2008) is used to calculate residue conservation.

For protein visualization, search result files were re-opened in PyMOL v2.4.1 (Schrödinger, 2010) (License invoice: #38352). Colored by secondary structure (ss) and illustrated with new images for each protein model with ligand, binding site (s), surface view, interior/exterior cavities, and pockets. Every PyMOL session was saved as an image in .pse* file format.

Molecular docking

After investigating each protein model, the Patchdock webserver was used to perform molecular docking with a silver nanoparticle (Ag^0) (Duhovny et al., 2002; Schneidman-Duhovny et

al., 2005). The ten most successful search results were selected and re-opened in PyMOL to capture figures of each 3D protein–metal interaction. To eliminate members surrounding each AgNP, "Polar Neighbor"-based measurements were chosen. A "Polar Neighbor" is defined as the center of any positive/negative atom within 3.5Å the distance of one bond from the provided selection. Subsequently, the amino acids closest to each AgNP were labeled using the "Polar Neighbors" (PNs) measurement wizard.

Molecular dynamic simulations (MDS)

Molecular dynamic simulations (MDS) were applied for one of the targeted proteins in this study (2b9y) and one of its ligands (FAD). This provides deep illustration of protein-ligand interaction. For both equilibration and run production GROMACS 2020.2 (Abraham et al., 2015) was used all MD calculations. Initially, the complex is solvated in a cubic box of TIP3P waters and then neutralization is achieved by adding Na^+ and Cl^- ions to the net atomic charge of the whole system by replacement of water molecules, randomly.

Also, CHARMM force field parameters for protein in CHARMM-GUI solution builder is used to generate input files for MD calculations (Jo et al., 2008). FAD's topology file is produced by CHARMM General Forcefield through ParamChem server (https://cgenff.umaryland.edu).

The CHARMM-GUI solution builder involves five steps. Firstly, the biomolecular coordinates of protein-ligand complex from RCSB website being read by CHARMM-GUI web portal . Secondly, solvation of the biomolecule is held by adding water molecules, then selecting the system's shape and dimensions.. After that, for system's neutralization, sodium and chloride ions are added. Thirdly, an approximation of the system is set using Periodic Boundary Conditions (PBC), where a unit cell is replicated in all directions. The atoms present inside the produced PBC box only are counted for simulation, while bad contacts are omitted by running short minimization. Non-bonded interactions were treated with a 12˚A cutoff distance and the neighbor searching list were buffered with the Verlet (Verlet, 1967) cutoff-scheme and the long-range electrostatic interactions were treated with the particle mesh Ewald (PME) method (Darden, 1993). The final two steps include equilibration of the system and production of simulation.

Two phases -*NVT* (No. of molecules, Volume and Temperature) and -*NpT* ((No. of molecules, Pressure and Temperature) ensembles for equilibrium is applied to ensure that the system has reached the desired temperature and pressure during MDS. The input files for equilibration and production are then downloaded. Some changes in the input files were made such as frequency of saving formed trajectory, number of steps of MD run, and calculation of binding energy, etc.

The system's energy is minimized by using steepest descent algorithm (5000 steps) before production of the simulation. The complex was then equilibrated for stabilizing its temperature and pressure by subjecting it to *NVT* and *NpT* ensemble and simulating for 125 ps at 300.15 K temperature using 400 kJ mol^{-1} nm^{-2} and 40 kJ mol^{-1} nm^{-2} positional restraints on the backbone and side chains, respectively.

Eventually, simulation run for 100 ns in *NpT* ensemble at 300.15 K and 1 bar is produced for the complex. To maintain the temperature and the pressure; Nose-Hoover thermostat (Braga & Travis, 2005) and similarly for maintaining Parrinello-Rahman barostat (Parrinello & Rahman, 1981) were used, respectively. The H-bonds were concluded using Linear constraint solver (LINCS) algorithm (Hess et al., 1997) from the inputs provided by CHARMM-GUI. The V-rescale thermostat at 300 K with a coupling constant of 1 ps was used. The trajectory was stored every 2 ps. The production stage for simulations of 100 ns in *NpT* assembly was performed.

Trajectory analysis

GROMACS utilities were used for the analysis of the MD simulations. The root mean square deviation (*RMSD*) of atom position for protein and ligand was calculated by fitting protein backbone atom with the *gmx_rms* subprogram. Also, root mean square fluctuations (*RMSF*) based on the protein *C-alpha* atoms were calculated using gmx_rmsf. The number of H- bonds were calculated (in-side the protein-ligand interface) with the gmx_hbond and the radius of gyration (*Rg*) of all atoms within the protein was calculated with the gmx_gyrate. The tool gmx_distance was used to calculate the center of mass distance between the protein and the ligand during the simulation. The VMD molecular graphics program was used for trajectory visualization and protein-ligand contact frequency analysis.

Binding free energy (MM/PBSA calculations)

The expected binding affinity is calculated using a GROMACS tool (g_mmpbsa) by performing Molecular Mechanics/Poisson–Boltzmann Surface Area (*MM*/*PBSA*). In general, the binding free energy of a complex (protein with ligand) in a solvent can be expressed as:

$$\Delta G_{binding} = \Delta G_{complex} - (\Delta G_{protein} + \Delta G_{ligand})$$

where, $\Delta G_{complex}$ is the total free energy of the protein–ligand complex, and $\Delta G_{protein}$ plus ΔG_{ligand} are the sum of free energies of the isolated protein and ligand in solvent, respectively. To decompose the binding energy, at first, ΔG_{polar} and $\Delta G_{non-polar}$ were separately calculated for each residue and were then summed up to obtain the contribution of each residue to the binding energy. Considering that g_mmpbsa only read the files of some specific GROMACS versions, the binary run input file (.tpr) required for *MM*/*PBSA* calculation through the g_mmpbsa was regenerated by GROMACS 5.1.4. The molecular structure file (.gro), topology file (.top) and MD-parameter file (.mdp) were necessary to generate the binary run input file, and all these files were produced from the MD process.

Results and Discussion

Generation of silver nanoparticles using AOry$_{17}$ filtrate

Figure 1 shows morphological characterization of *Aspergillus oryzae*. The colony color is olive green, vesicles are globose and sub-globose, uni- and bi-serriate, and conidia are echinulate.

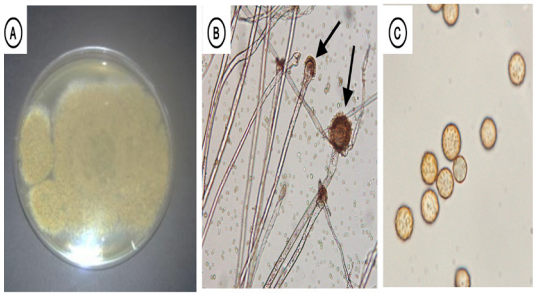

Fig. 1. Morphological characterization of *Aspergillus oryzae*; (A) Colony color, (B) Conidiophores and vesicles and (C) Rough conidia

Silver nanoparticles were detected using UV-vis spectrophotometer (*JENWAY*1750) after 24 h. The peak shows OD at 440 nm with 1.5 absorbance (Fig. 2A). Figure 2B shows the change in filtrate color, which occurs due to the surface plasmon resonance (*SPR*) of metallic nanoparticles. In this phenomenon the light reflects from NPs' surface and can be detected in the visible region (Kelly et al., 2003). The TEM micrograph shows that the particles are spherical in shape (Fig. 2C) and to obtain particles size distribution, ninety-one particles were measured in nm scale and analysed using OriginPro version 2023. Using the Gaussian equation for peak fit (y = y0+A/(w*sqrt(pi/(4*ln(2))))*exp(-4*ln(2)*(x-xc)^2/w^2)) showed that the majority of particles are in 13.6 ± 2.2 nm size range (Fig. 2D).

Protein modeling and docking

In this report, we present the homology modeling of five extracellular proteins produced by *A*. *oryzae*. In addition, we detected the ligands and residues of each protein. This is the first comparative proteome analysis of an in silico molecular docking of silver nanoparticles with the filamentous fungus *A*. *oryzae*'s extracellular proteins. Our analysis revealed that PNs at a maximum distance of 3.5 Å from a silver atom play a crucial role in protein-silver nanoparticle interaction. In contrast to previous studies that reported this reduction activity could be carried out by any reducing biomolecule associated with electron transfer during the transformation of NADPH/NADH to $NADP^+/NAD^+$ (Ahmad et al., 2003; Anil Kumar et al., 2007; Thakkar et al., 2010; Gudikandula et al., 2017), this study demonstrates that a specific biomolecule is responsible for this reduction activity. From docking results, we report that FAD-dependent oxidoreductase is a species-specific reducing agent that involved in protein-silver nanoparticle interaction.

All presented models were identified through the Phyre2 web server with a confidence score of 100. Our analysis showed that the highest number of solutions with PNs found with nine out of ten solutions in Alkaline protease, partial gi|BAA00258 (Fig. 3). Also, the highest number of total PNs in result solutions is found to be 13 in the same protein and in FAD-dependent oxidoreductase gi|BAK26560. Examining docked solutions, showed that only 3 out of 5 proteins detected PNs interfering with their binding sites, with one measurement for Alkaline protease, partial gi|BAA00258 and Leucine aminopeptidase A gi|Q2U1F3. The most interesting part is the six measurements that were detected associated with the FAD binding site of FAD-dependent oxidoreductase, as will be explained later in this research.

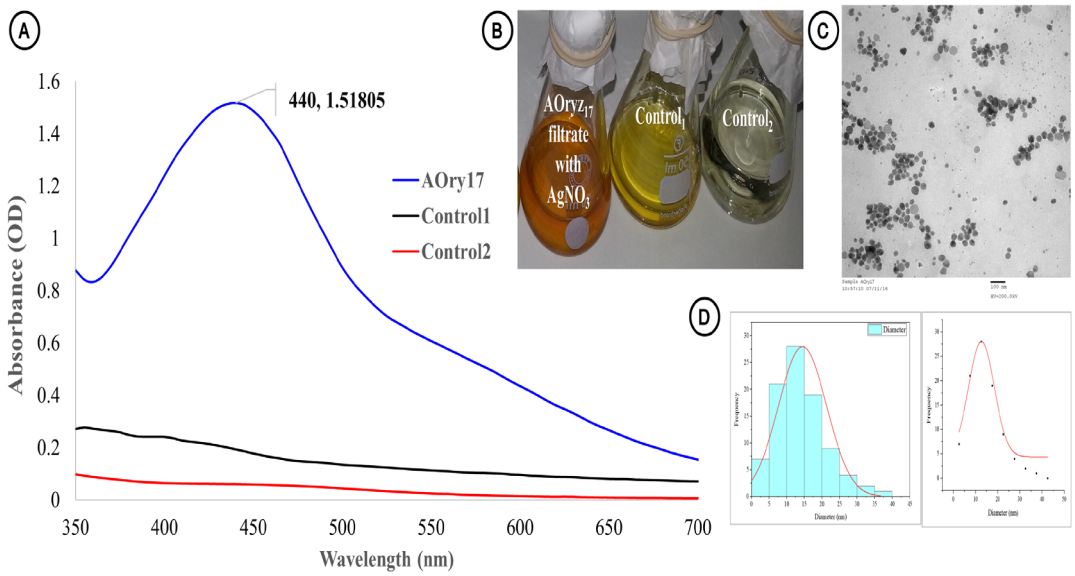

Fig. 2. Detection and characterization of formed AgNPs; (A) UV-vis absorption spectrum of AgNPs using $AOry_{17}$ filtrate after 24h at 28C, (B) Change in the color of filtrate solution, (C) TEM micrograph of AgNPs showing their morphology, (D) Histogram of particles' size distribution.f AgNPs showing their morphology and (D) Histogram of particles' size distribution

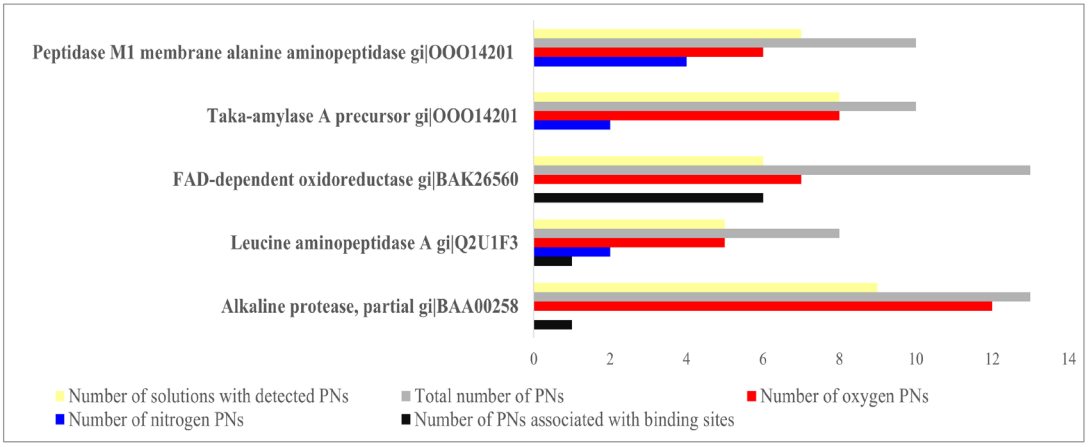

Fig. 3. A comparison between the five proteins under study, in terms of number of solutions with detected PNs, total number of PNs, number of oxygen PNs, nitrogen PNs, and number of PNs associated with binding sites

Polar neighbors

Docking of silver nanoparticles with each protein yields a multitude of solutions. Only the top ten solutions for each protein were individually visualized in PyMOL (50 solutions, 10 per protein). Using the "Measurement" wizard to detect PNs, only 32 of 50 solutions revealed the presence of PNs containing an oxygen or nitrogen atom. Red sticks denote an oxygen atom (v dw radius 1.52 Å). Furthermore, blue sticks denote a nitrogen atom (v dw radius 1.55 *Å) that may or may not possess a formal charge (O^{-1} and N^{+1}, respectively) (O^{0} and N^{0}).*

Peptidase M1 membrane alanine aminopeptidase [Aspergillus oryzae], gi|OOO14201

Phyre2 template for peptidase M1 membrane alanine aminopeptidase is 4fytA; MAMMOTH average value for structural search confidence data from structural library search is 45.112 InE. The first identified cluster contains 25 ligands (ZN heterogens in the binding site), and 5 residues (HIS-318, GLU-319, HIS-322, GLU-341, and ALA-344) were predicted to serve as binding sites (Fig. 4).

Membrane alanine aminopeptidase peptidase

M1 is a member of the metallopeptidase family. Most metalloproteases contain a HEXXH motif, which is reported in crystallographic studies and forms part of the metal-binding site. H represents histidine, E represents glutamate, and X represents any amino acid (Rawlings & Barrett, 1995). The motif in this protein is HEALH, as depicted in Fig. 4 by the sticks HIS-318, GLU-319, ALA-321, LEU-320, and HIS-322.

The docking of 10 solutions is depicted in Fig. 4B. Nine of 10 solutions demonstrated that silver atoms are captured in cavities or pockets at various sites, while 7 of 10 solutions demonstrated the presence of PNs between 2.4 and 3.4 Å away from each Ag^0.

Solutions 2 and 7 contained polar nitrogen atoms with a (+1) formal charge (namely, NZ). There were two measurements of PNs in solutions 6, 9, and 10, with either two oxygen atoms or one nitrogen atom and another oxygen atom, but no formal charges were detected.

Taka-amylase A precursor [Aspergillus oryzae], gi|BAA00336

The second protein modeled is taka-amylase A precursor [*Aspergillus oryzae*] built using the 2taaA Phyre2 template, 2taaA. Cluster 1 was identified with 24 ligands of CA (heterogeny in binding site) and only two amino acids (asparagine (ASN_{142}) and aspartate (ASP_{196}) as binding sites (Fig. 5).

Only 8 of the top 10 solutions labeled in solid surface representation (50 % transparency) and have PNs ranging from 0.5 to 3.4. In contrast, two of the solutions (3 and 4) exhibited no PNs. In solutions 5 and 9, the atoms NZ in residue LYS_{333} and NH1 in residue ARG_{42}, respectively, exhibit a positive charge (+1) (Fig. 5B).

FAD-dependent oxidoreductase [Aspergillus oryzae], gi|BAK26560

The Phyre2 homology modeling template is 2b9y. Mammoth searches of structural libraries yield an average lnE value of 37,064. Cluster 1 was identified, with 25 ligands containing FAD as a heterogens within 37 binding sites (Fig. 6B).

Furthermore, in 6 of 10 solutions, polar neighbors were detected at 3.0 to 3.5 Å from each AgNP (Fig. 7). Oxygen atoms were found as PNs in all solutions (red). Solution seven reveals that PNs are six FAD residues, namely 458, 461, 462, 463, 469, and 474. The first and sixth solutions contain two PNs: TRP-341 and ALA-348 for AG docking_1 and THR-71 and GLU-223 for AG docking_6. The docking solutions 3, 5, and 10 demonstrated PNs with Asp-108, ASN-120, and GLN-274, respectively (Fig. 7).

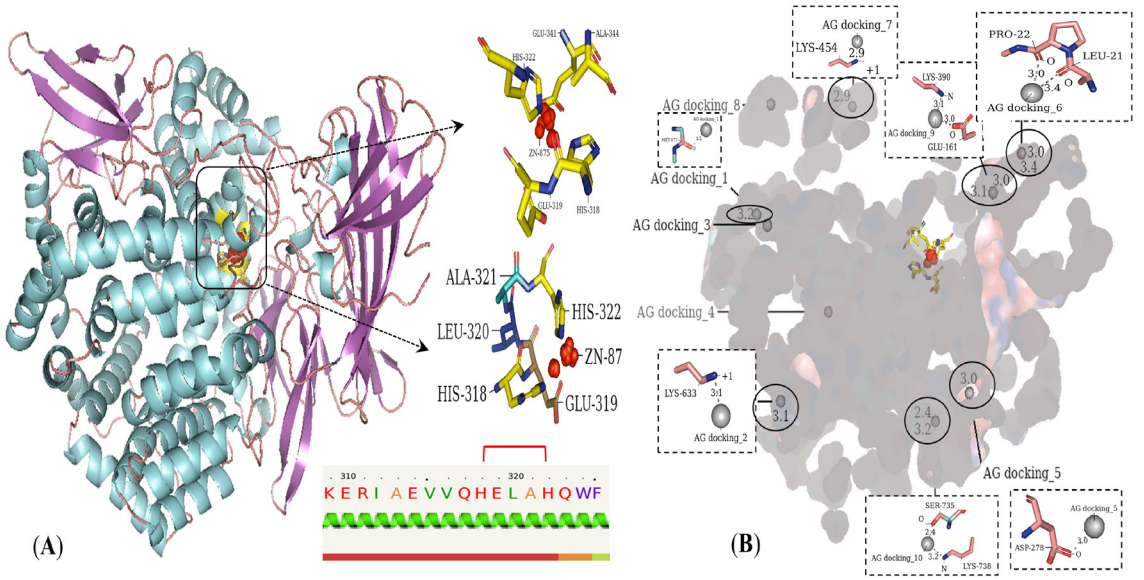

Fig. 4. Structural view of homology modeling for peptidase M1 membrane alanine aminopeptidase in a complex with a ligand site; (A) Cartoon representation according to secondary structure, five binding sites with ZN heterogeneity within each, and the motif HEXXH and (B) Measurements of PN in the top 10 solutions for docking AgNP with the first protein [Cavities and pockets depict a protein carrying 10 AgNPs in various positions. The stick representation of detected PNs in solutions 2, 7, 6, 9, and 10 are magnified]

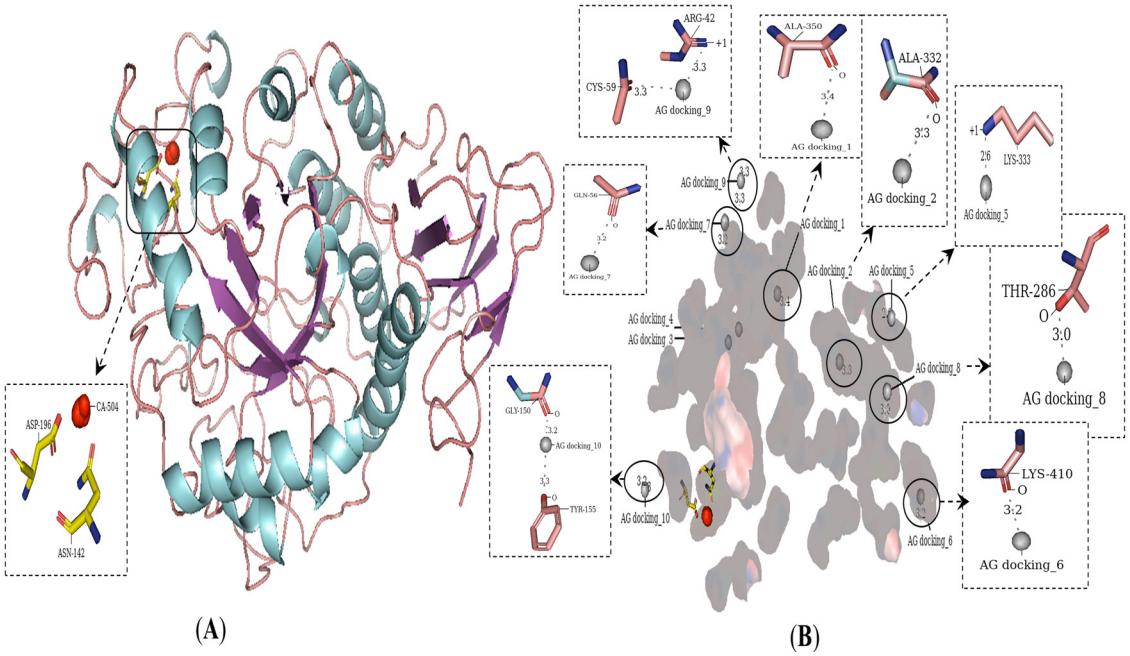

Fig. 5. Structural representation of Taka-amylase model prediction; (A) Illustration of the structure and detected binding site and (B) Cavities and pockets (culled) representations containing the leading 10 options [Measurement of polar neighbors is used to represent eight solutions as sticks]

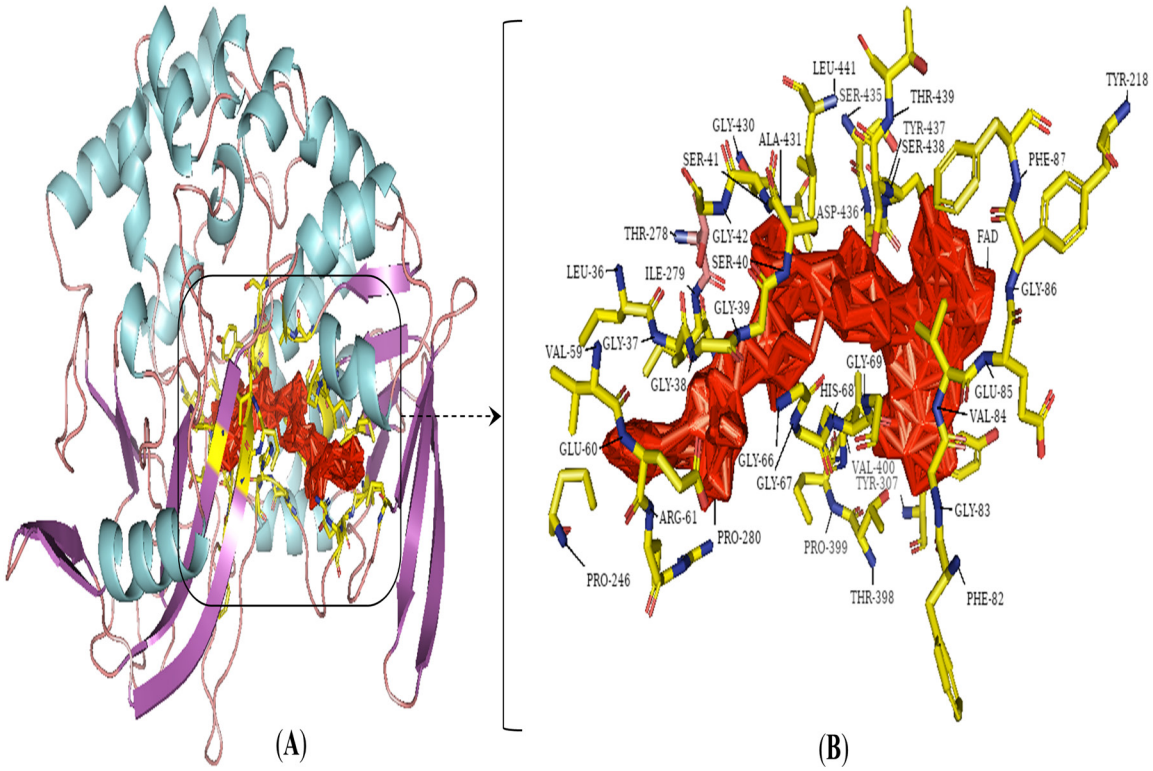

Fig. 6. Homology modeling of FAD-dependent oxidoreductase [*Aspergillus oryzae*]; (A) Representation of a cartoon based on secondary structure and (B) Thirty-seven binding sites and FAD heterogeneity within each binding site

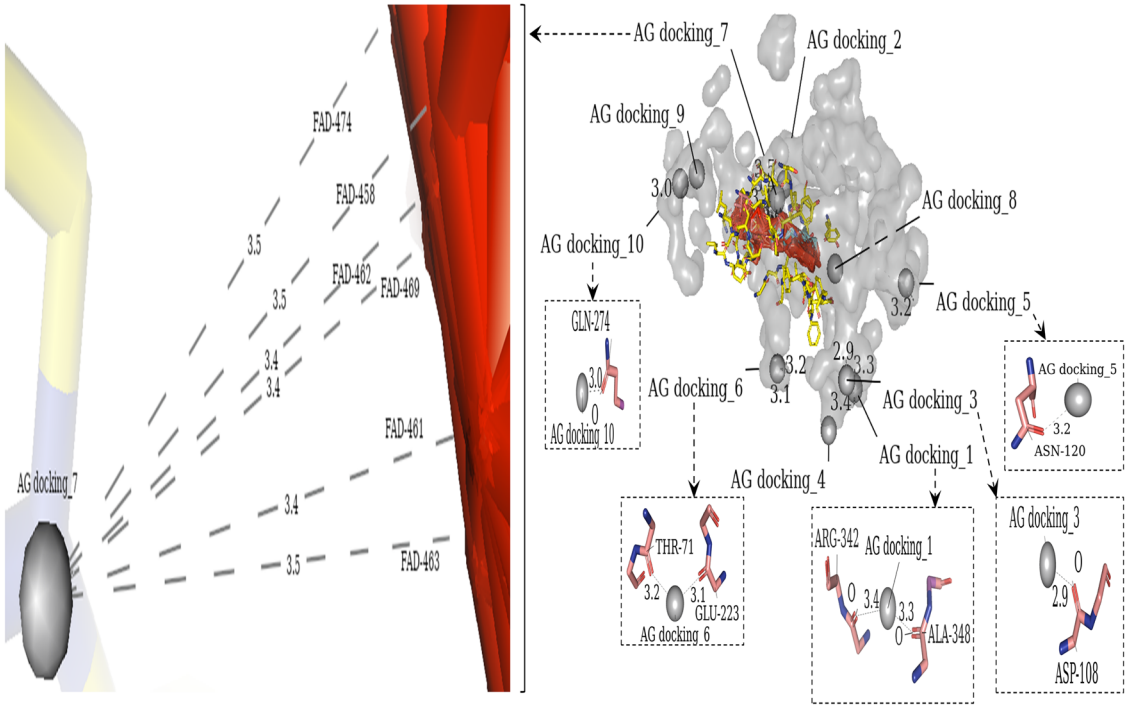

Fig. 7. Black solid surface protein representation shows docked silver atoms and measurements labeled for the top 10 docking solutions [Sticks representation of six solutions for docking were magnified]

AG docking_7 depicts the highest number of PNs recorded for all proteins. This finding demonstrates the essential role of FAD in the reaction of silver ions (Ag^{+}_{aq}) with fungal extract's aqueous solution. At the nanoscale, the presence of extracellular FAD-dependent oxidoreductase provides enough electrons to convert silver ions (Ag^{+}_{aq}) into solid silver (Ag^{0}_{s}).

According to molecular biology, the FAD-dependent oxidoreductase family of proteins is a member of the FAD-dependent oxidoreductase family. Both NADPH and FAD are coenzymes that participate in reversible oxidation and reduction reactions. As demonstrated in this study, as electron carriers, NAD^{+} and FAD^{+} participate in the breakdown of large molecules such as silver nitrate. Consequently, both can donate electrons to diverse biochemical reactions within the cell. The only distinction between these two coenzymes is that FAD can accept two hydrogen atoms while NAD can only accept one. Hulikere & Joshi (2019) explained the role of NADPH in reducing Ag^{+} ions into Ag^{0} atoms in the cell-free extract of the endophytic fungus *Cladosporium cladosporiodes*; however, in this study, we report FAD-dependent oxidoreductase as the primary reducing protein for forming AgNPs. This is also in accordance with Rai et al. (2021) who reported that although there are extremely a lot of organisms that can produce metal nanoparticles intra/extracellularly, but this reducing capability is a species-specific reaction.

Leucine aminopeptidase A [Aspergillus oryzae RIB40], gi|Q2U1F3

The Phyre2 template for this protein is 6zepA. Furthermore, the structural search average MAMMOTH score was lnE:32.4. 45 ligands with ZN heterogens present in eight predicted binding sites at ARG-50, HIS-176, ASP-195, ASP-196, GLU-233, GLU-234, ASP-261, and HIS-343 were identified in cluster 1 (Fig. 8).

Five of the top 10 solutions contained PNs with distances ranging from 2.6 to 3.5 Å AG docking 3, 4, 6, 7, and 8 are depicted in Fig. 8 with various PNs. One of the eight binding sites, GLU-233, exhibits a formal charge of (−1) in solution 7. Ag docking 3 with OH in TYR-323 and OE in GLU-245 is observed to have two PNs. Ag docking 4 and 6 revealed a nitrogen atom as a PN in ILE-349 and ARG-62, respectively.

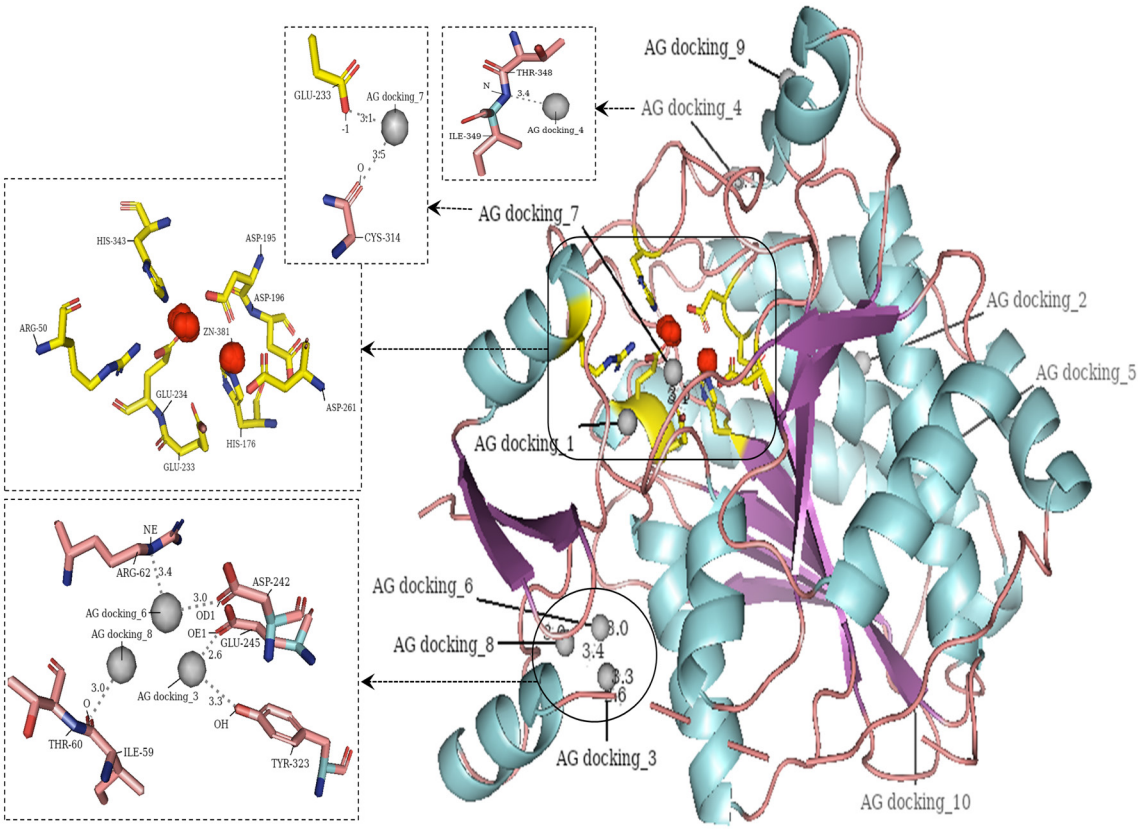

Fig. 8. Homology modeling of leucine aminopeptidase A [*Aspergillus oryzae* RIB40]; Representation of a cartoon based on secondary structure. Anticipated binding sites and heterogeny of ZN [Ten solutions docking measurement, including detection of PNs]

Alkaline protease, partial [Aspergillus oryzae], gi|BAA00258

Homology modeling for this protein was constructed using a 3f7oB Phyre2 template. The average MAMMOTH score of 34.9 identified cluster 1 with 11 ligands. Two predicted binding sites, ALA-179 and ASP-202, with 11 CA counts as heterogeneity (Fig. 9).

In 8 out of 10 solutions, polar neighbors with an oxygen atom are found between 2.5 and 3.4 Å away from silver atoms (figure not shown). At TYR-240, ALA-61, THR-23, LEU-260, and GLU-226, only one PN atom was detected in AG docking 1, 3, 5, 6, and 9, respectively. AG docking_7 revealed two PNs with SER-127 and ASN-246, whereas AG docking_8 revealed two PNs with only SER-103. AG docking_10 revealed that an oxygen atom had three PNs, ASP-202, VAL-201, and LYS-199.

Molecular dynamic simulations (MDS)

Root mean square deviation (RMSD)

Among the five proteins selected for analysis in this study, FAD dependent oxidoreductase is further analyzed for protein-ligand complex, 100 ns all-atom molecular dynamic simulations computed by GROMACS tool. The secondary structure stability and protein conformational changes upon ligand binding were tested by analyzing 100 ns MD trajectories for RMSD of the protein backbone and RMSF of α-C atoms of the protein. The RMSD plot (Fig. 10A) depicts that the RMSD of unbound ligand (FAD) showed sudden fluctuations in the range 38–48 ns. The mean RMSD of unbound protein (~ 0.1 nm) is higher than the RMSD of unbound FAD. This indicates that upon ligand binding, protein dynamicity and stability increase significantly for the complex for 100 ns.

Solvent accessible surface area (SASA)

To test the conformational changes upon ligand binding, Solvent accessible surface area (SASA) was plotted to show the 100 ns trajectory of 2b9y-FAD complex. The SASA value increased through the simulation which indicate the structure expansion which leads to increased solvent access of the surface area of protein is efficiently stabilized (Fig. 10B).

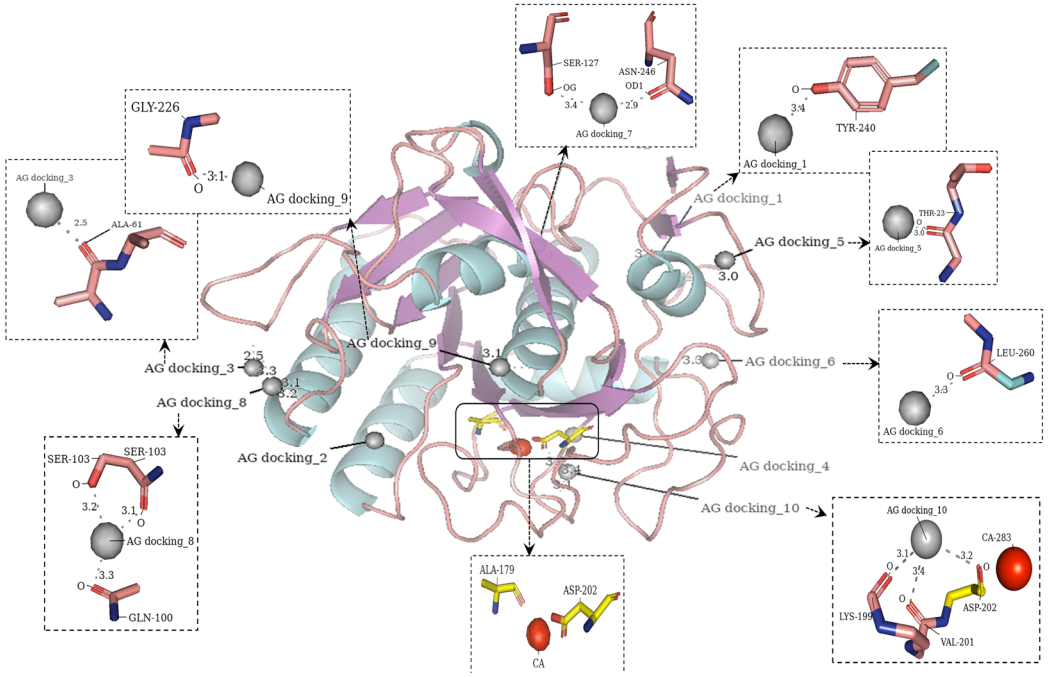

Fig. 9. Homology modeling of gi|BAA00258 (Alkaline protease, partial [*Aspergillus oryzae*]). Cartoon illustration with secondary structure coloring (ss), and 50% transparency. Two predicted binding sites, ALA-179 and ASP-202, with 11 counts of CA representing heterogeny. Eight solutions are represented in sticks depicts PNs

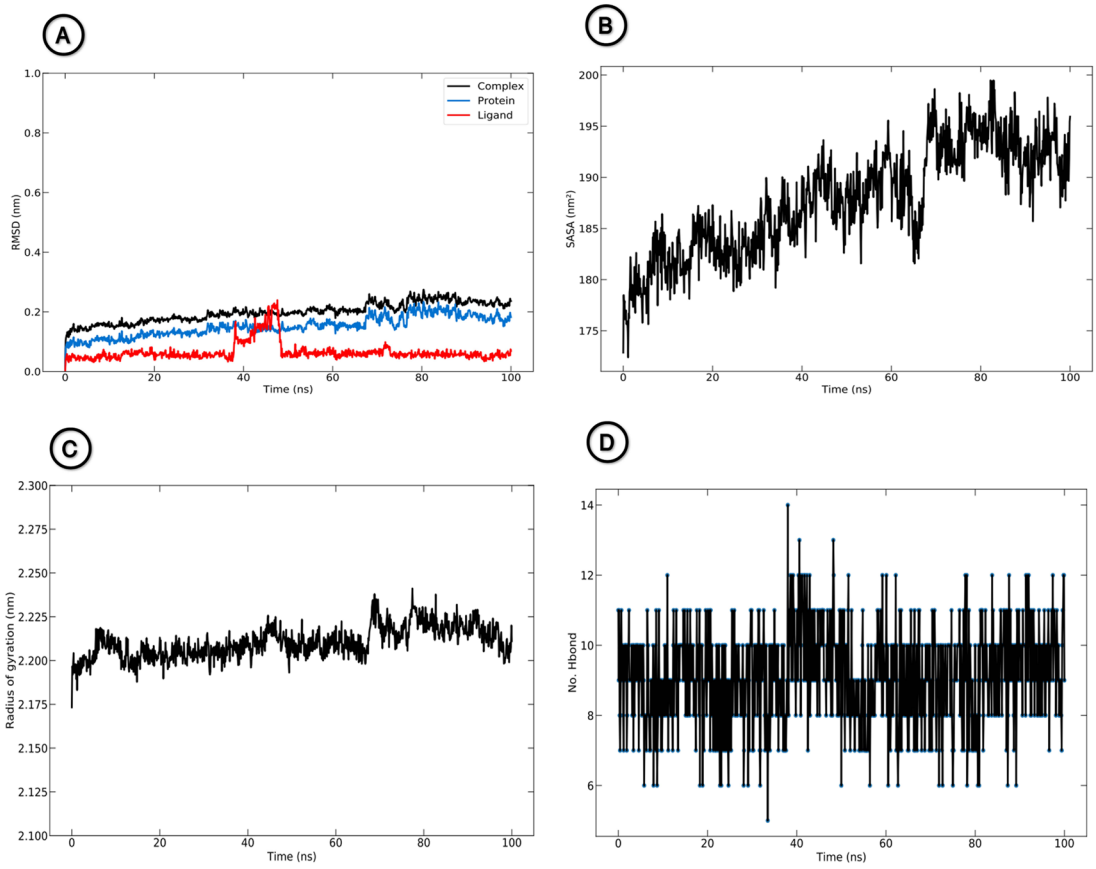

Fig. 10. Molecular dynamic simulations of 2b9y-FAD complex; (A) Root mean square deviation (RMSD), (B) Solvent accessible surface area (SASA), (C) Radius of gyration (Rg) and (D) Hydrogen bonding

Radius of gyration (Rg)

Radius of gyration is calculated to figure out the protein's compactness variation during the simulation. The Rg was stable from the initial simulation up to 68 ns (2.157-2.200 nm). Then slightly increased to 2.238 nm at 70 ns during the remaining simulation (Fig. 10C). The trajectory of simulation for complex shows its compactness through the simulation which indicates the stabilization of 2b9y through ligand (FAD) binding.

Hydrogen bonding

The binding affinity between protein and ligand contributes to polar interactions between them. Hence, intermolecular H- bond formation between protein and ligand were calculated from the 100 ns trajectory. Figure 10D shows persistency in H- bonds between protein and ligand. Hence, hydrogen bonding significantly affects the binding energy of the 2b9y-FAD complex.

Conclusion

The biogenesis of silver nanoparticles by fungi is well-documented, but the precise mechanism of this biological process has not yet been determined. A large number of questions regarding this protein–metal interaction can be answered using computational techniques. Docking and homology modeling clarify how these proteins function as reducing or capping agents during the formation of silver nanoparticles. The most prevalent participants in this bioprocess among extracellular protein families are oxidoreductase family members. The FAD-dependent oxidoreductase is the primary extracellular protein produced by *A. oryzae* that interacts with silver nanoparticles. Although all binding sites were predicted and labeled, only 3 out of 50 solutions were discovered to be associated with AgNPs. At the FAD, GLU-233, and ASP-202 binding sites of FAD-dependent oxidoreductase, Leucine aminopeptidase, and alkaline protease, a silver nanoparticle interacts in a polar neighbor. Therefore, the interaction between silver nanoparticles and protein binding sites is not exclusive. Each docking solution clarifies the potential of these proteins to function as capping agents for at least the 10 most effective solutions for each protein. Molecular dynamic simulations confirmed the stability of 2b9y-FAD complex system, hence the essential role for FAD as a ligand in 2b9y protein's function.

Data availability: Amino acid sequences are available to download from NCBI. Files from Mascot, 3DLigandSite, Phyr2, Patchdock, and PyMOL sessions are not included with this manuscript but may be requested from the authors.

Disclosure statement: The authors declare that they have no conflict of interest in the publication.

Acknowledgment: The authors thank the Egyptian Knowledge Bank (EKB) for providing language editing of our manuscript through ';enago' Copyediting service. Thanks to Prof. Dr. Aly Abo-Amer, head of Botany and Microbiology Department, Sohag University, for all support and facilities he offered during performing this research.

References

Abraham, M.J., Murtola, T., Schulz, R., Páll, S., Smith, J.C., Hess, B., Lindahl, E. (2015) GROMACS: High performance molecular simulations through multi-level parallelism from laptops to supercomputers. *SoftwareX*, **1**, 19-25.

Ahmad, A., Mukherjee, P., Senapati, S., Mandal, D., Khan, M.I., Kumar, R., Sastry, M. (2003) Extracellular biosynthesis of silver nanoparticles using the fungus *Fusarium oxysporum*. *Colloids and surfaces B: Biointerfaces*, **28**(4), 313-318.

Anil Kumar, S., Abyaneh, M.K., Gosavi, S.W., Kulkarni, S.K., Pasricha, R., Ahmad, A., Khan, M.I. (2007) Nitrate reductase-mediated synthesis of silver nanoparticles from $AgNO_3$. *Biotechnology Letters*, **29**(3), 439-445.

Bérdy, J. (2005) Bioactive microbial metabolites. *The Journal of Antibiotics*, **58**(1), 1-26.

Bhimba, B.V., Gurung, S., Nandhini, S.U. (2015) Silver nanoparticles synthesized from marine fungi *Aspergillus oryzae*. *International Journal of ChemTech Research,* **7**(01), 68-72.

Braga, C., Travis, K.P. (2005) A configurational temperature Nosé-Hoover thermostat. *The Journal of Chemical Physics*, **123**(13), 134101.

Capra, J.A., Singh, M. (2008) Characterization and prediction of residues determining protein functional specificity. *Bioinformatics*, **24**(13), 1473-1480.

Darden, T., York, D., Pedersen, L. (1993) Particle mesh Ewald: An N. log (N) method for Ewald sums in large systems. *The Journal of Chemical Physics*, **98**(12), 10089-10092.

Duhovny, D., Nussinov, R., Wolfson, H.J. (2002) Efficient unbound docking of rigid molecules. In: *International Workshop on Algorithms in Bioinformatics*. Springer, Berlin, Heidelberg, pp. 185-200.

Gudikandula, K., Vadapally, P., Charya, M.S. (2017) Biogenic synthesis of silver nanoparticles from white rot fungi: Their characterization and antibacterial studies. *OpenNano*, **2**, 64-78.

Guilger-Casagrande, M., Lima, R.D. (2019) Synthesis of silver nanoparticles mediated by fungi: a review. *Frontiers in Bioengineering and Biotechnology*, **7**, 287.

Gupta, R.K., Kumar, V., Gundampati, R.K., Malviya, M., Hasan, S.H., Jagannadham, M.V. (2017) Biosynthesis of silver nanoparticles from the novel strain of *Streptomyces* Sp. BHUMBU-80 with highly efficient electroanalytical detection of hydrogen peroxide and antibacterial activity. *Journal of Environmental Chemical Engineering*, **5**(6), 5624-5635.

Hess, B., Bekker, H., Berendsen, H.J., Fraaije, J.G. (1997) LINCS: a linear constraint solver for molecular simulations. *Journal of Computational Chemistry*, **18**(12), 1463-1472.

Hulikere, M.M., Joshi, C.G. (2019) Characterization, antioxidant and antimicrobial activity of silver nanoparticles synthesized using marine endophytic fungus- *Cladosporium cladosporioides*. *Process Biochemistry*, **82**, 199-204.

Jo, S., Kim, T., Iyer, V.G., Im, W. (2008) CHARMM-GUI: a web-based graphical user interface for CHARMM. *Journal of Computational Chemistry*, **29**(11), 1859-1865.S.

Kelley, L.A., Mezulis, S., Yates, C.M., Wass, M.N., Sternberg, M.J. (2015) The Phyre2 web portal for protein modeling, prediction and analysis. *Nature Protocols*, **10**(6), 845-858.

Kelly, K.L., Coronado, E., Zhao, L.L., Schatz, G.C. (2003) The optical properties of metal nanoparticles: the influence of size, shape, and dielectric environment. *The Journal of Physical Chemistry B*, **107**(3), 668-677.

Liang, Y., Pan, L., Lin, Y. (2009) Analysis of extracellular proteins of *Aspergillus oryzae* grown on soy sauce koji. *Bioscience, Biotechnology, and Biochemistry*, **73**(1), 192-195.

Loo, Y.Y., Rukayadi, Y., Nor-Khaizura, M.A.R., Kuan, C.H., Chieng, B.W., Nishibuchi, M., Radu, S. (2018) In vitro antimicrobial activity of green synthesized silver nanoparticles against selected gram-negative foodborne pathogens. *Frontiers in Microbiology*, **9**, 1555.

Matsushita-Morita, M., Furukawa, I., Suzuki, S., Yamagata, Y., Koide, Y., Ishida, H., Takeuchi, M., Kashiwagi, Y., Kusumoto, K.-I. (2010) Characterization of recombinant prolyl aminopeptidase from *Aspergillus oryzae*. *Journal of Applied Microbiology*, **109**(1), 156-165.

Mehra, R.K., Winge, D.R. (1991) Metal ion resistance in fungi: molecular mechanisms and their regulated expression. *Journal of Cellular Biochemistry*, **45**(1), 30-40.

Ortiz, A.R., Strauss, C.E., Olmea, O. (2002) MAMMOTH (matching molecular models obtained from theory): an automated method for model comparison. *Protein Science*, **11**(11), 2606-2621.

Parrinello, M., Rahman, A. (1981) Polymorphic transitions in single crystals: A new molecular dynamics method. *Journal of Applied Physics*, **52**(12), 7182-7190.

Rai, M., Kon, K., Ingle, A., Duran, N., Galdiero, S., Galdiero, M. (2014) Broad-spectrum bioactivities of silver nanoparticles: the emerging trends and future prospects. *Applied Microbiology and Biotechnology*, **98**(5), 1951-1961.

Rai, M., Bonde, S., Golinska, P., Trzcińska-Wencel, J., Gade, A., Abd-Elsalam, K.A., Shende, S., Gaikwad, S., Ingle, A.P. (2021) *Fusarium* as a novel fungus for the synthesis of nanoparticles: Mechanism and applications. *Journal of Fungi*, **7**(2), 139.

Rawlings, N.D., Barrett, A.J. (1995) [13] Evolutionary families of metallopeptidases. In: "*Methods in Enzymology*", (Vol. 248, pp. 183-228). Academic Press.

Schneidman-Duhovny, D., Inbar, Y., Nussinov, R., Wolfson, H.J. (2005) PatchDock and SymmDock: servers for rigid and symmetric docking. *Nucleic Acids Research*, **33**(suppl_2), W363-W367.

Schrödinger, L.L.C. (2010) The PyMOL molecular graphics system. Version 2.4.1.

Tarafdar, J.C., Raliya, R. (2013) Rapid, low-cost, and ecofriendly approach for iron nanoparticle synthesis using *Aspergillus oryzae* TFR9. *Journal of Nanoparticles*, (2013), 1-4.

Thakkar, K.N., Mhatre, S.S., Parikh, R.Y. (2010) Biological synthesis of metallic nanoparticles. *Nanomedicine: Nanotechnology, Biology and Medicine*, **6**(2), 257-262.

Verlet, L. (1967) Computer" experiments" on classical fluids. I. Thermodynamical properties of Lennard-Jones molecules. *Physical Review*, **159**(1), 98.

Warcup, J.H. (1950) The soil-plate method for isolation of fungi from soil. *Nature*, **166**(4211), 117-118.

Wass, M.N., Kelley, L.A., Sternberg, M.J. (2010) 3DLigandSite: predicting ligand-binding sites using similar structures. *Nucleic Acids Research*, **38**(suppl_2), W469-W473.

Yadav, A., Kon, K., Kratosova, G., Duran, N., Ingle, A.P., Rai, M. (2015) Fungi as an efficient mycosystem for the synthesis of metal nanoparticles: progress and key aspects of research. *Biotechnology Letters*, **37**(11), 2099-2120.

Zhang, Y., Skolnick, J. (2005) TM-align: a protein structure alignment algorithm based on the TM-score. *Nucleic Acids Research*, **33**(7), 2302-2309.

تصميم نماذج بالتماثل لخمسة بروتينات تنتج خارجيا لفطر أسبرجلس أوريزي حاسوبيا، والإلتحام بجسيمات الفضة النانوية.

هدي عبدالحميد، مروة عبيدالله
قسم النبات و الميكروبيولوجي – كلية العلوم – جامعة سوهاج- سوهاج- مصر.

يساعد إستخدام الأساليب الحسابية لبناء نموذج بروتيني لدعم النتائج التجريبية في الإجابة على عدد كبير من الأسئلة حول الآليات الكامنة وراء العمليات العلمية المختلفة. تتمثل إحدى الطرق الأكثر دقة المتاحة حاليًا في اكتشاف متماثل لتسلسل حمض أميني معين لاستخدامه كنموذج لبناء نموذج بروتيني مجهول. في هذا البحث، نقدم تحضير 4.5 نانومتر من جسيمات الفضة النانوية بغستخدام رشيح فطر أسبرجلس أوريزي خارج الخلية و نماذج لخمسة بروتينات مستهدفة خارج الخلية بناءا علي التماثل البروتيني، بالإضافة إلى التنبؤ لكل موقع نشط لكل بروتين، بالتماثل البروتيني أيضا. بالإضافة إلى ذلك ، يتم تقييم جسيمات الفضة النانوية التي تلتصق بالبروتينات الخمسة بالبرمجة. وفقًا للنتائج ، إحتوى 32 فقط من أفضل 50 محلولًا لكل بروتين على الأكسجين القطبي أو ذرات النيتروجين المجاورة. إحتوت سبعة من الحلول الخمسين لأكسيدوريداكتيز ديبيندانت FAD على أكبر عدد من الجيران القطبيين الذين يمكن إكتشافهم (ستة قياسات). تدعم هذه النتيجة الفرضية الداعمة بأن البروتينات الفطرية خارج الخلية تلعب دورًا مهمًا في تغطية الجسيمات النانوية الفضية في مواقع مختلفة ومنع تراكم وترسيب هذه الجسيمات. من خلال النمذجة المتجانسة والإلتحام، نكشف لأول مرة عن التفاعل بين أكسيدوريداكتيز ديبيندانت FAD وجسيمات الفضة النانوية.